Biological Psychiatry: Celebrating 50 Years

Priority Communication

Early Correction of *N*-Methyl-D-Aspartate Receptor Function Improves Autistic-like Social Behaviors in Adult *Shank2*$^{-/-}$ Mice

Changuk Chung, Seungmin Ha, Hyojin Kang, Jiseok Lee, Seung Min Um, Haidun Yan, Ye-Eun Yoo, Taesun Yoo, Hwajin Jung, Dongwon Lee, Eunee Lee, Seungjoon Lee, Jihye Kim, Ryunhee Kim, Yonghan Kwon, Woohyun Kim, Hyosang Kim, Lara Duffney, Doyoun Kim, Won Mah, Hyejung Won, Seojung Mo, Jin Yong Kim, Chae-Seok Lim, Bong-Kiun Kaang, Tobias M. Boeckers, Yeonseung Chung, Hyun Kim, Yong-hui Jiang, and Eunjoon Kim

ABSTRACT

BACKGROUND: Autism spectrum disorder involves neurodevelopmental dysregulations that lead to visible symptoms at early stages of life. Many autism spectrum disorder–related mechanisms suggested by animal studies are supported by demonstrated improvement in autistic-like phenotypes in adult animals following experimental reversal of dysregulated mechanisms. However, whether such mechanisms also act at earlier stages to cause autistic-like phenotypes is unclear.

METHODS: We used *Shank2*$^{-/-}$ mice carrying a mutation identified in human autism spectrum disorder (exons 6 and 7 deletion) and combined electrophysiological and behavioral analyses to see whether early pathophysiology at pup stages is different from late pathophysiology at juvenile and adult stages and whether correcting early pathophysiology can normalize late pathophysiology and abnormal behaviors in juvenile and adult mice.

RESULTS: Early correction of a dysregulated mechanism in young mice prevents manifestation of autistic-like social behaviors in adult mice. *Shank2*$^{-/-}$ mice, known to display *N*-methyl-D-aspartate receptor (NMDAR) hypofunction and autistic-like behaviors at postweaning stages after postnatal day 21 (P21), show the opposite synaptic phenotype—NMDAR hyperfunction—at an earlier preweaning stage (~P14). Moreover, this NMDAR hyperfunction at P14 rapidly shifts to NMDAR hypofunction after weaning (~P24). Chronic suppression of the early NMDAR hyperfunction by the NMDAR antagonist memantine (P7–P21) prevents NMDAR hypofunction and autistic-like social behaviors from manifesting at later stages (~P28 and P56).

CONCLUSIONS: Early NMDAR hyperfunction leads to late NMDAR hypofunction and autistic-like social behaviors in *Shank2*$^{-/-}$ mice, and early correction of NMDAR dysfunction has the long-lasting effect of preventing autistic-like social behaviors from developing at later stages.

Keywords: Autism, Memantine, NMDA receptor, SHANK2, Synapse, Treatment

https://doi.org/10.1016/j.biopsych.2018.09.025

Autism spectrum disorder (ASD), characterized by social deficits and repetitive behaviors, exhibits a strong genetic influence. While the number of candidate ASD-risk genes is rapidly increasing (1), our understanding of the underlying mechanisms has lagged, partly because of the intrinsic heterogeneity and complexity of causal mechanisms in different brain regions at different developmental times.

Many ASD-related mechanisms suggested by animal studies are supported by demonstrated improvement in autistic-like phenotypes in adult animals following experimental reversal of dysregulated mechanisms (2–11). However, whether such mechanisms also act at earlier stages to cause autistic-like phenotypes is unclear (12,13).

SHANK is a family of postsynaptic scaffolding proteins known to regulate excitatory synapse development and function (14,15) and involved in various psychiatric disorders, including ASD and Phelan-McDermid syndrome (4,7,16,17). SHANK2, the second member of the family also known as PROSAP1, has also been implicated in ASD and other disorders, including intellectual disability, developmental delay, and schizophrenia (18–31).

More recently, studies on mice lacking SHANK2 in the whole brain or specific cell types have further enhanced our understanding of the normal functions of SHANK2 as well as ASD-related pathophysiology (32–45). For example, mice lacking exons 6 and 7 and exon 7of *Shank2* display autistic-like behavioral abnormalities that are associated with altered *N*-methyl-D-aspartate receptor (NMDAR) function (37,38).

More specifically, *Shank2*$^{-/-}$ mice with exons 6 and 7 deletion show decreased NMDAR-mediated synaptic currents

SEE COMMENTARY ON PAGE 530

 ISSN: 0006-3223

and NMDAR-dependent synaptic plasticity (38). Importantly, the treatment of adult *Shank2*$^{-/-}$ mice with D-cycloserine (NMDAR agonist) rapidly normalizes social interaction, suggesting that suppressed NMDAR function may underlie the social deficits. However, it remains unclear whether the NMDAR hypofunction observed in adult *Shank2*$^{-/-}$ mice (exons 6 and 7) also acts at early stages to play important roles in the development of social deficits.

In the present study, we found an increase in NMDAR function at an earlier stage (~postnatal day 14, or P14), which sharply contrasts with the decreased NMDAR function at ~P21. Importantly, suppression of the early NMDAR hyperfunction by the treatment of *Shank2*$^{-/-}$ mice with memantine (NMDAR antagonist) during the P7 to P21 period normalized NMDAR function and social interaction at juvenile (~P28) as well as adult (~P56) stages. These results suggest that early NMDAR hyperfunction induces NMDAR hypofunction and social deficits at later stages, and that early correction of NMDAR function has long-lasting effects.

METHODS AND MATERIALS

Animals

Shank2$^{-/-}$ mice lacking the exons 6 and 7 of the *Shank2* gene have been previously reported (38). *Shank2*$^{-/-}$ mice lacking exon 7 (37) and exon 24 (33) have also been previously reported. All mutant and their wild-type (WT) littermates of *Shank2*$^{-/-}$ mice lacking exons 6 and 7 were generated on and backcrossed to a C57BL/6N background for >20 generations. *Shank2*$^{-/-}$ mice lacking exons 6 and 7 under a different background (C57BL/6J) were generated by backcrossing the original mice in the genetic background of C57BL/6N with C57BL/6J for more than six generations. *Shank2*$^{-/-}$ mice lacking exon 7 have been previously published (37) and backcrossed to and maintained in a C57BL/6J background for more than five generations.

Further information on methods is available in the Supplement.

RESULTS

Distinct Transcriptomic Profiles in *Shank2*$^{-/-}$ Mouse Brains at P14 and P25

Mice lacking SHANK2/PROSAP1 (*Shank2*$^{-/-}$ mice; exons 6 and 7; global deletion) display autistic-like social deficits that are rapidly improved by acute D-cycloserine (NMDAR agonist) treatment at juvenile and adult stages (38). However, excitatory synaptogenesis in mice is most active during the first 3 postnatal weeks (46), and expression levels of SHANK2 protein in the whole brain peak at ~P14 (Figure 1A), although SHANK2 messenger RNA levels did not show a similar pattern (Figure 1B).

We thus sought to identify phenotypes that are most prominent at P14 through comparative RNA sequencing transcriptomic analysis of WT and *Shank2*$^{-/-}$ mouse brains at P21, a stage around weaning when active synaptogenesis is largely completed (Supplemental Table S1). We found 16 differentially expressed genes (false discovery rate < .05, fold change > 2.0) in six pairs of naïve WT versus *Shank2*$^{-/-}$ mice at P14, and 35 differentially expressed genes at P25 (Supplemental Table S2). However, because the small number of the identified differentially expressed genes did not yield

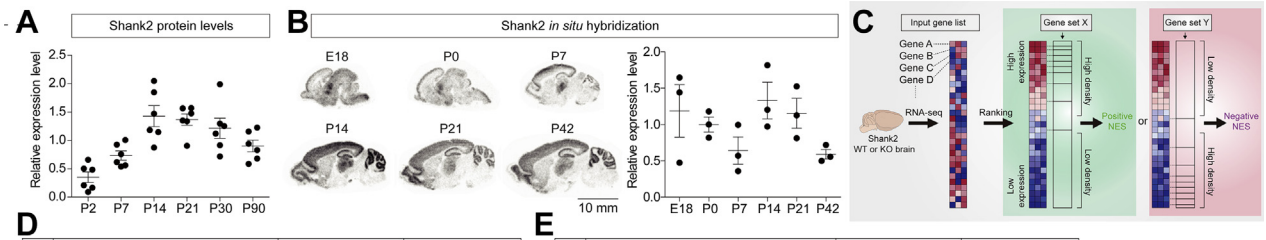

D

C5CC synapse related	Gene set name	P14 [KO/WT] NES	P14 [KO/WT] FDR p-value	P25 [KO/WT] NES	P25 [KO/WT] FDR p-value
	Postsynapse	4.447	<0.001***	1.370	0.602
	Excitatory synapse	4.106	<0.001***	1.074	0.831
	Synaptic membrane	4.028	<0.001***	1.146	0.760
	Postsynaptic membrane	3.687	<0.001***	1.302	0.647
	Neuronal postsynaptic density	2.921	<0.001***	0.911	0.917

E

C2 NMDAR related	Gene set name	P14 [KO/WT] NES	P14 [KO/WT] FDR p-value	P25 [KO/WT] NES	P25 [KO/WT] FDR p-value
	Long term depression	4.304	<0.001***	0.679	0.947
	Long term potentiation	3.024	<0.001***	1.080	0.627
	Activation of NMDA receptor...	2.205	0.018*	-0.877	0.878
	Post_NMDA receptor activation events	2.009	0.042*	-0.845	0.892

Figure 1. Distinct transcriptomic profiles in *Shank2*$^{-/-}$ mouse brains at postnatal day 14 (P14) and P25. **(A)** Levels of SHANK2 proteins in whole mouse brains increase during postnatal days, reaching a plateau at ~P14. For quantification, SHANK2 signals at each developmental stages were normalized to those of α-tubulin and also to the average values of each age group (n = 6 male mice for each stage). **(B)** Levels of SHANK2 messenger RNAs in the mouse brain during development, revealed by in situ hybridization of sagittal sections. The limited correlation between SHANK2 protein and messenger RNA levels might be attributable to the fact that the transcripts are differentially translated or that the in situ images do not cover the whole brain. For quantification, SHANK2 signals normalized to the brain area at each developmental stage were normalized to the average values of each age groups (n = 3 male mice for each stage). E18 indicates embryonic day 18. Scale bar = 10 mm. **(C)** A schematic of gene set enrichment analysis. The direction (positive and/or negative) and amplitude of enrichments reflect the extent to which the genes in a target gene set fall at the top (positive) or bottom (negative) of the ranked input gene list. **(D)** Gene set enrichment analysis using knockout/wild-type (KO/WT)-P14 and KO/WT-P25 gene lists from *Shank2*$^{-/-}$ mice and target gene sets in the C5-CC category (gene ontology_cellular component). Positive and negative normalized enrichment score (NES) values, accounting for the degree of overrepresentation at the top or bottom of a ranked list, are indicated in green and violet, respectively. (n = 6 mice for WT and KO at P14 and P25. ***False discovery rate [FDR] < .001.) (See Supplemental Table S4 for details.) **(E)** Gene set enrichment analysis using KO/WT-P14 and KO/WT-P25 gene lists from *Shank2*$^{-/-}$ mice and *N*-methyl-D-aspartate receptor (NMDAR)-related gene sets in the C2-all category. "Activation of NMDA receptor …" indicates "Activation of NMDA receptor upon glutamate binding and postsynaptic event." (n = 6 mice for WT and KO at P14 and P25. *FDR < .05, ***FDR < .001.) (See Supplemental Table S3 for details.)

significant gene ontology terms or pathways, we next performed gene set enrichment analysis (software.broadinstitute.org/gsea/) (Figure 1C), which aims to achieve unbiased results by testing the enrichment of a list of ranked, whole genes, rather than a subset above an arbitrary cutoff (fold-change or significance), in precurated gene sets (47,48).

The two lists of genes from *Shank2*$^{-/-}$ versus WT (knockout [KO]/WT) mice at P14 and P25, ranked by differential expression, were distinctly enriched for a large number of target gene sets in the C2 category (curated gene sets) (Supplemental Table S3). Importantly, the top 10 enriched target gene sets for P14 and P25 were largely distinct, and in the case of the four overlapping gene sets associated with ribosome/translational terms, the directions of enrichments were opposite (Supplemental Figure S1).

Additional gene set enrichment analysis using target gene sets in the C5 category (gene ontology) revealed that the KO/WT-P14, but not KO/WT-P25, gene list was enriched for gene sets associated with excitatory postsynaptic compartments, including excitatory synapse, postsynaptic membrane, and postsynaptic density (Figure 1D, Supplemental Figure S2, Supplemental Table S4).

Because *Shank2*$^{-/-}$ mice show autistic-like behaviors accompanied by reduced NMDAR function (38), we examined NMDAR-related enrichments. The KO/WT-P14 but not KO/WT-P25 gene list was enriched for gene sets associated with NMDAR activation and NMDAR-dependent synaptic plasticity (long-term potentiation and long-term depression) (Figure 1E, Supplemental Figure S2). Collectively, these results suggest that *Shank2* deletion in mice leads to distinct transcriptomic changes at P14 and P25.

Reversal of NMDAR Function in *Shank2*$^{-/-}$ Mice During P14 and P25

Based on these results, we next measured excitatory synaptic transmission mediated by NMDARs and α-amino-3-hydroxy-5-methyl-4-isoxazolepropionic acid receptors (AMPARs) in the hippocampus, a brain region implicated in ASD (49–51), in *Shank2*$^{-/-}$ mice at P14 and P25. We found an increase in the ratio of NMDAR- to AMPAR-mediated synaptic transmission at Schaffer collateral (SC)–CA1 pyramidal synapses at ∼P14, as compared with that at WT synapses (Figure 2A; all electrophysiology data summarized in Supplemental Table S5).

In contrast, basal synaptic transmission, mainly mediated by AMPARs, and paired-pulse ratio (a measure of presynaptic release probability) were normal at *Shank2*$^{-/-}$ SC-CA1 synapses (Supplemental Figure S3). In addition, there were no changes in miniature excitatory postsynaptic currents (mEPSCs), mediated by AMPARs, and miniature inhibitory

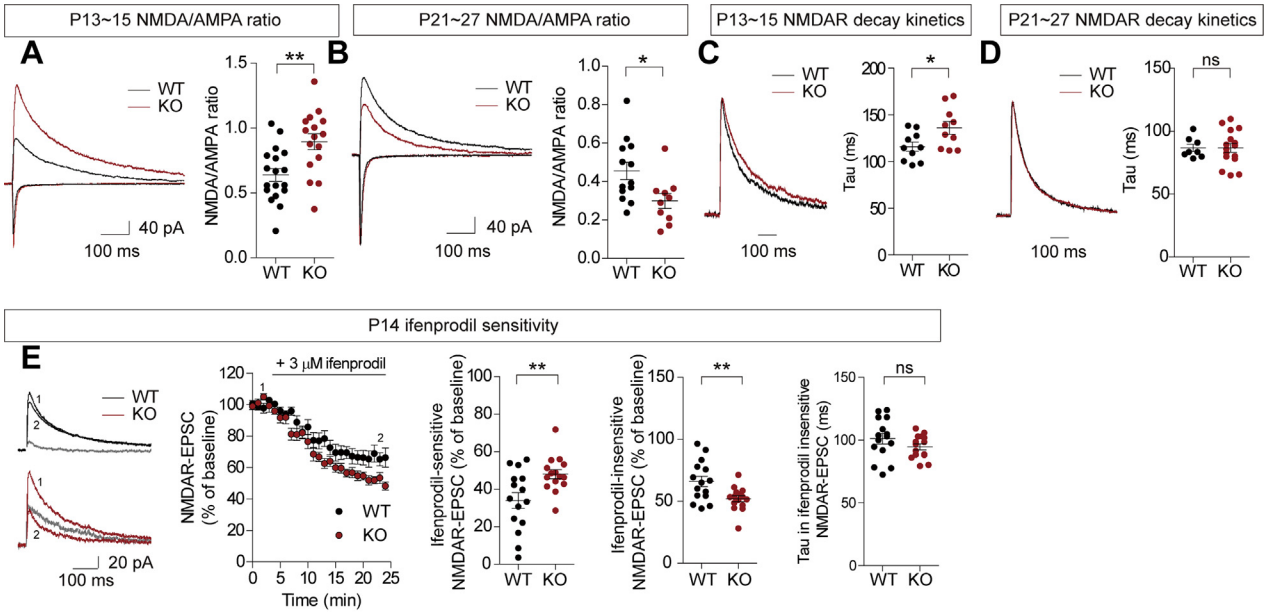

Figure 2. Reversal of *N*-methyl-D-aspartate receptor (NMDAR) function in the *Shank2*$^{-/-}$ hippocampus during postnatal day 14 (P14) and P25. **(A, B)** NMDAR function is enhanced at *Shank2*$^{-/-}$ Schaffer collateral (SC)-CA1 synapses at ∼P13 to P15, but reduced at ∼P21 to P27, as shown by the NMDA–α-amino-3-hydroxy-5-methyl-4-isoxazolepropionic acid (AMPA) ratio. (n = 18 neurons from 11 mice for wild-type [WT] and 16 neurons from 11 mice for knockout [KO; *Shank2*$^{-/-}$] at P13–P15, and 13 neurons from 8 mice for WT and 10 neurons from 6 mice for KO at P21–P27; $^{*}p < .05$, $^{**}p < .01$; Student's t test. See Supplemental Table S5 for the summary of electrophysiology results and Supplemental Table S6 for statistical details.) **(C, D)** Reduced decay of NMDAR currents at *Shank2*$^{-/-}$ SC-CA1 synapses at ∼P13 to P15, but not at ∼P21 to P27. (n = 10 neurons from 4 mice for WT and 10 neurons from 4 mice for KO at P13–P15, and 8 neurons from 6 mice for WT and 16 neurons from 9 mice for KO at P21–P27; $^{*}p < .05$, not significant [ns]; Student's t test.) **(E)** NMDAR currents at P14 *Shank2*$^{-/-}$ SC-CA1 synapses are more sensitive to ifenprodil (GluN2B antagonist) relative to those at WT synapses, which, in combination with the data in panel **(A)**, predicts a ∼2.07-fold and ∼1.06-fold increases in ifenprodil-sensitive GluN2B and ifenprodil-insensitive GluN2A components, respectively. Numbers 1 and 2 in WT and KO traces indicate NMDAR currents before and after ifenprodil treatment, respectively, and gray lines in WT and KO traces indicate ifenprodil-sensitive (or GluN2B-dependent) component. Note that the decay constant of the residual NMDAR–excitatory postsynaptic currents (EPSCs) lacking the GluN2B component is comparable between genotypes. (n = 15 neurons in 9 mice for WT and 15 neurons in 7 mice for KO; $^{**}p < .01$; Student's t test.)

postsynaptic currents in *Shank2*$^{-/-}$ CA1 pyramidal neurons (Supplemental Figure S4). These results suggest that NMDAR-mediated, but not AMPAR-mediated, synaptic transmission is increased at P14 *Shank2*$^{-/-}$ SC-CA1 synapses.

At ~P24 (P21–P27), however, the NMDA-AMPA ratio at *Shank2*$^{-/-}$ SC-CA1 synapses was decreased, as compared with that at WT synapses (Figure 2B), consistent with the results from the previous study (38). This study also demonstrated normal basal transmission at *Shank2*$^{-/-}$ SC-CA1 synapses and normal mEPSCs in *Shank2*$^{-/-}$ CA1 pyramidal neurons. These results suggest that NMDAR-mediated, but not AMPAR-mediated, synaptic transmission is reduced at P25 *Shank2*$^{-/-}$ SC-CA1 synapses.

This age-dependent shift in NMDAR function was similar in male and female mice (Supplemental Figure S5). In addition, the increased NMDAR function at P14 in *Shank2*$^{-/-}$ mouse synapses involved mainly the GluN2B subunit of NMDARs, as supported by the slower decay kinetics of NMDAR currents in the *Shank2*$^{-/-}$ mice at P14, but not at ~P24 (Figure 2C, D), and the higher sensitivity of the currents to the GluN2B-specific inhibitor ifenprodil, as compared with those in WT mice (Figure 2E).

In addition to the hippocampus, layers II and III pyramidal neurons in the medial prefrontal cortex (mPFC), another ASD-related brain region (52), showed a similar switch of NMDAR function: an increased NMDA-AMPA ratio at *Shank2*$^{-/-}$ mouse synapses at P14, but a decreased ratio at ~P24 (Supplemental Figure S6).

When mEPSCs were measured in these mPFC neurons, the amplitude of mEPSCs in P14 *Shank2*$^{-/-}$ mouse neurons was normal (Supplemental Figure S7A), suggesting, together with the increased NMDA-AMPA ratio, that NMDAR-mediated transmission is selectively increased. The mEPSC frequency, however, was decreased in these *Shank2*$^{-/-}$ mouse mPFC neurons, which, together with the normal paired pulse ratio (Supplemental Figure S7B), suggests that excitatory synapse number is decreased in P14 *Shank2*$^{-/-}$ mouse mPFC neurons.

These results collectively suggest that *Shank2* deletion induces a rapid temporal switch of NMDAR function from hyper- to hypofunction across the period of P14 to P24 in the hippocampus and mPFC.

To explore the mechanisms underlying the distinct NMDAR function at P14 and P25 *Shank2*$^{-/-}$ mouse synapses, we examined total and phosphorylation levels of NMDAR subunits in *Shank2*$^{-/-}$ mouse brains. Phosphorylation, but not total, levels of NMDAR subunits (GluN2B-Ser1303 and GluN1-Ser896), which have been shown to regulate surface and synaptic trafficking of GluN2B (53), were increased at P14 but decreased at P21 (Supplemental Figure S8A, B).

Other glutamate receptor (GluA and mGluR) subunits were largely normal in total levels in both P14 and P21 *Shank2*$^{-/-}$ mouse brains. In addition, signaling molecules were also largely normal, with moderate changes in the phosphorylation of extracellular signal-regulated kinase 1, cAMP-response element binding protein, and p38 (Supplemental Figure S8C, D).

Early Memantine Normalizes NMDAR Function in Juvenile and Adult *Shank2*$^{-/-}$ Mice

We next tested whether the early NMDAR hyperfunction at P14 is causally associated with NMDAR hypofunction at later stages by chronically suppressing NMDAR hyperfunction at ~P14 (P7–P21) and examining NMDAR phenotypes in juvenile (~P28) and adult (~P56) *Shank2*$^{-/-}$ mice.

We first tested whether early memantine treatment rescues NMDAR function in adult *Shank2*$^{-/-}$ mice. Young *Shank2*$^{-/-}$ mice orally administered the NMDAR antagonist memantine (20 mg/kg, twice daily) for 2 weeks before weaning (P7–P21) showed normalized NMDA-AMPA ratio at hippocampal SC-CA1 synapses in *Shank2*$^{-/-}$ mice at P25 to P31 (Figure 3A), without affecting mEPSCs (Supplemental Figure S9).

In addition, early memantine treatment rescued NMDAR-dependent long-term potentiation induced by high-frequency stimulation at SC-CA1 synapses in *Shank2*$^{-/-}$ mice, both immediately after memantine treatment (P25–P31) and at an adult stage (>P56) (Figure 3B,C), with no difference between male and female mice (Supplemental Figure S10). In contrast, early memantine treatment had no effect on long-term potentiation at WT SC-CA1 synapses at either stage.

Early memantine treatment for a shorter period (P7–P14) could rescue the NMDA-AMPA ratio even at P14, without affecting mEPSCs (Figure 3D, Supplemental Figure S11), which is indicative of a strong and immediate effect of early memantine treatment on the normalization of NMDAR function. These results collectively suggest that early memantine treatment induces immediate and long-lasting normalization of NMDAR function.

Early Memantine Improves Social Interaction in Juvenile and Adult *Shank2*$^{-/-}$ Mice

We next tested whether early memantine treatment can rescue abnormal behaviors in *Shank2*$^{-/-}$ mice at later (juvenile and adult) stages. Early memantine treatment (20 mg/kg, twice daily; P7–P21) significantly improved social interaction of juvenile (P28–P35) *Shank2*$^{-/-}$ mice in the direct interaction test (Figure 4A, B). Social isolation or weaning of mice before direct social-interaction tests had no effect on the results (Supplemental Figure S12). In contrast, early memantine treatment did not affect social interaction in WT mice (Figure 4B). Memantine also improved social interaction of adult (~P56) *Shank2*$^{-/-}$ mice in the three-chamber test (54) (Figure 4C–E, Supplemental Figure S13), which is indicative of a long-lasting effect.

When we tested olfactory function and social hierarchy, known to significantly affect social interaction in mice (55–60), olfactory function was similar between genotypes, as reported previously (38), whereas *Shank2*$^{-/-}$ mice were submissive to WT mice in both tube and urine tests (Supplemental Figure S14A–C), suggesting that *Shank2* deletion affects social hierarchy in mice. This submissiveness, however, did not correlate with social interaction at the individual mouse level (Supplemental Figure S14D–G). In addition, this submissiveness was not improved by early memantine treatment (Supplemental Figure S14B, C).

Early memantine treatment modestly improved hyperactivity in adult *Shank2*$^{-/-}$ mice in the open-field test (Supplemental Figure S15A–C). However, increasing habituation to a new environment eliminated the drug effect (Supplemental Figure S15D–G). In addition, the hyperactivity of *Shank2*$^{-/-}$ mice in a familiar environment was not normalized by early memantine treatment (Supplemental Figure S16). Early

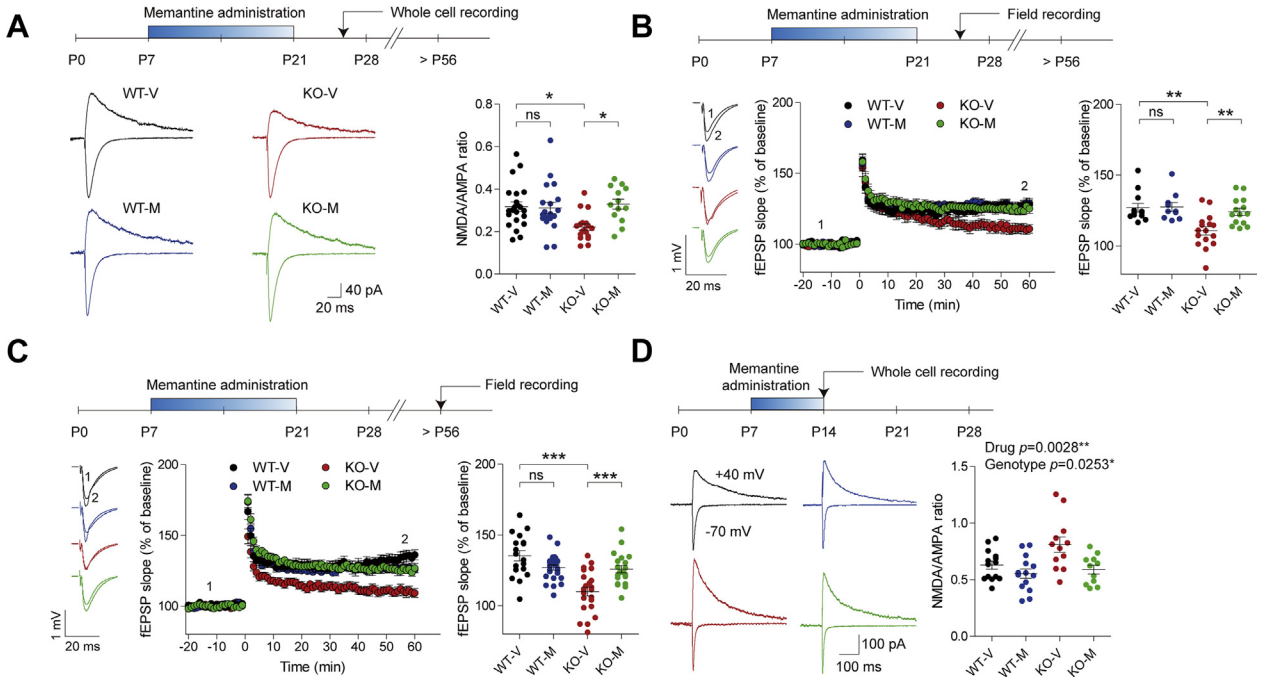

Figure 3. Early memantine treatment normalizes *N*-methyl-D-aspartate receptor (NMDAR) function in the juvenile and adult *Shank2*$^{-/-}$ hippocampus. **(A)** Early memantine treatment (postnatal day [P]7–P21) normalizes the NMDA–α-amino-3-hydroxy-5-methyl-4-isoxazolepropionic acid (AMPA) ratio at juvenile (~P25–P31) *Shank2*$^{-/-}$ Schaffer collateral (SC)-CA1 synapses. Young *Shank2*$^{-/-}$ mice were orally administered memantine (20 mg/kg) twice daily for 2 weeks during the P7 to P21 period followed by measurements of NMDA-AMPA ratio at ~P25 to P31. (n = 22 neurons from 9 mice for wild-type vehicle [WT-V], 19 neurons from 6 mice for WT-memantine [M], 18 neurons from 9 mice for knockout [KO]-V, and 13 neurons from 3 mice for KO-M; *$p < .05$; two-way analysis of variance with Holm-Sidak test.) **(B, C)** Early memantine treatment (P7–P21) normalizes long-term potentiation induced by high-frequency stimulation at juvenile (~P25–P31) **(B)** and adult (>P56) **(C)** *Shank2*$^{-/-}$ SC-CA1 synapses. Numbers 1 and 2 indicate field excitatory postsynaptic potential (fEPSP) slopes during the baseline and last 5-minute recordings, respectively. (Juvenile, n = 12 slices from 6 mice for WT-V, 10 slices from 5 mice for WT-M, 16 slices from 8 mice for KO-V, and 14 slices from 8 mice for KO-M; adult, n = 18 slices from 9 mice for WT-V, 25 slices from 12 mice for WT-M, 23 slices from 9 mice for KO-V, and 20 slices from 7 mice for KO-M; **$p < .01$, ***$p < .001$, not significant [ns]; two-way analysis of variance with Holm-Sidak test.) **(D)** Early memantine treatment for a shorter period (P7–P14; 20 mg/kg oral/day) normalizes the NMDA-AMPA ratio at ~P15 at *Shank2*$^{-/-}$ SC-CA1 synapses. (n = 14 neurons from 8 mice for WT-V, 14 neurons from 4 mice for WT-M, 12 neurons from 7 mice for KO-V, and 11 neurons from 6 mice for KO-M; *$p < .05$, **$p < .01$; two-way analysis of variance.)

memantine treatment did not rescue other behavioral abnormalities of *Shank2*$^{-/-}$ mice, including reduced ultrasonic vocalizations, enhanced repetitive behaviors, and anxiolytic-like behavior (Supplemental Figure S17).

Early D-Cycloserine or Late Memantine Fails to Normalize Social Interaction in *Shank2*$^{-/-}$ Mice

Importantly, treating *Shank2*$^{-/-}$ mice with D-cycloserine instead of memantine from P7 to P21 did not improve social interaction or hyperactivity, which is similar to the results from WT mice (Figure 5A–C, Supplemental Figure S18). Intriguingly, early memantine-treated WT mice showed decreased NMDAR function at ~P21 to P25, as shown by the decreased NMDA-AMPA ratio and normal mEPSC amplitude (Supplemental Figure S19); the mEPSC frequency was also reduced, likely through compensatory mechanisms. These results suggest that artificially elevated NMDAR function in WT mice during an early stage (P7–P21) is sufficient to induce NMDAR hypofunction in juvenile mice (~P21–P25) but not abnormal behaviors in adult mice.

Treating *Shank2*$^{-/-}$ mice with memantine at a late stage (P25–P39) failed to improve social interaction or hyperactivity (Figure 5D–F, Supplemental Figure S20). Acute memantine treatment at P56 also failed to correct social interaction or hyperactivity (Supplemental Figure S21). These results collectively suggest that early NMDAR hyperfunction in *Shank2*$^{-/-}$ mice should be corrected early and in the right direction.

Developmental Switch of NMDAR Function Is Not Observed in Other *Shank2*$^{-/-}$ Mutant Mice

We next tested whether the temporal shift in NMDAR function in our *Shank2*$^{-/-}$ mice also occurred in other *Shank2*-mutant mouse lines (33,37). *Shank2*$^{-/-}$ mice lacking exon 24 (*Shank2*-dEx24) showed reduced NMDAR function at P21, similar to the reported NMDAR hypofunction at ~2 to 4 months (33), but normal NMDAR function at P14 (Supplemental Figure S22). In addition, *Shank2*$^{-/-}$ mice lacking exon 7 (*Shank2*-dEx7) showed enhanced NMDAR function at P21, similar to the reported NMDAR hyperfunction at ~P24 (37), but normal NMDAR function at P14 (Supplemental Figure S23).

Moreover, a switch in the background of our *Shank2*$^{-/-}$ mice lacking exons 6 and 7 from C57BL/6N to C57BL/6J had no effect on the reduced NMDAR function at ~P24 (Supplemental Figure S24). Therefore, temporal patterns of NMDAR functions in different *Shank2*$^{-/-}$ mouse lines seem to be distinct.

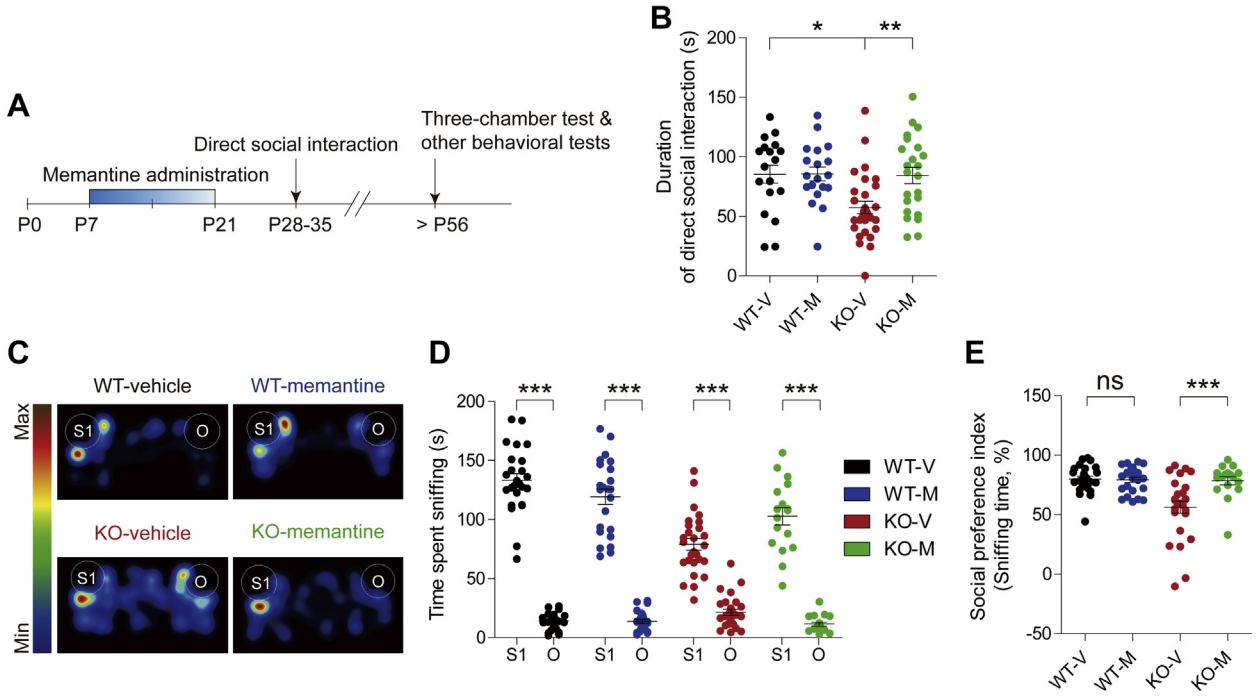

Figure 4. Early memantine treatment improves social interaction in juvenile and adult *Shank2*$^{-/-}$ mice. **(A)** Schematic depiction of early memantine treatment. Young *Shank2*$^{-/-}$ mice were orally administered memantine (20 mg/kg) twice daily for 2 weeks from postnatal day (P)7 to P21, followed by measurements of social interactions at juvenile (P28–P35) and adult (P56) stages. **(B)** Early memantine treatment improves social interaction of juvenile *Shank2*$^{-/-}$ mice (P28–P35), as indicated by time spent in social interaction in the direct interaction test. (n = 18 mice for wild-type vehicle [WT-V], 19 mice for WT-memantine [M], 29 mice for knockout (KO)-V, and 23 mice for KO-M; $^{*}p < .05$, $^{**}p < .01$; two-way analysis of variance with Bonferroni test.) **(C–E)** Early memantine treatment improves social interaction of adult *Shank2*$^{-/-}$ mice (> P56), as indicated by time spent sniffing stranger mouse/object (S1/O) **(D)** and the social preference index based on sniffing time (the numerical difference between the time spent sniffing S1 and O divided by their sum × 100) **(E)** in the three-chamber test. [n = 25 mice for WT-V, 24 mice for WT-M, 27 mice for KO-V, and 17 mice for KO-M; $^{***}p < .001$; Student's t test for WT-V and WT-M in panel **(D)**, Wilcoxon matched-pairs signed rank test for KO-V and KO-M in panel **(D)**, and Mann-Whitney U test in panel **(E)**; two-way analysis of variance was not performed because the social preference index is a normalized value]. Max, maximum; min, minimum; ns, not significant.

Lastly, we sought to identify additional molecular differences between *Shank2*$^{-/-}$ mice lacking exons 6 and 7 and those lacking exon 7, which show opposite NMDAR functions at ~P21 (37,38) and minimally overlapping transcriptomic profiles (34). Intriguingly, *Shank2*$^{-/-}$ mice lacking exons 6 and 7 had undetectable levels of the shorter SHANK2A splice variant, whereas *Shank2*$^{-/-}$ mice lacking exon 7 had markedly increased (~sixfold) levels of the SHANK2A variant, while both mouse types had similarly decreased levels of the longer SHANK2B splice variant (Supplemental Figures S25 and S26). Whether this differential splice variant expression leads to differences in NMDAR function remains to be determined. Our molecular modeling, however, predicted that the short peptide (57 aa-long) produced from the SHANK2B splice variant in *Shank2*-dEx7 mice by protein truncation may form a structure that partly mimics the *N*-terminal region of the SHANK2 PDZ domain and may compete with the normal SHANK2 PDZ domain for binding to the *C*-terminal PDZ-binding domains of GKAPs/SAPAPs in a dominant-negative manner (Supplemental Figure S27).

DISCUSSION

Our study provides early NMDAR hyperfunction at ~P14 as a causal mechanism for the NMDAR hypofunction and social deficits in *Shank2*$^{-/-}$ mice at juvenile (~P28) and adult (~P56) stages. In support of this, *Shank2*$^{-/-}$ mice display a rapid reversal of NMDAR function during P14 and P21 in the hippocampus (Figure 2, Supplemental Figures S3–S5) as well as in the mPFC (Supplemental Figures S6 and S7). Importantly, early memantine treatment (P7–P21) normalizes NMDAR function and social interaction without affecting other behaviors at juvenile and adult stages (Figures 3 and 4, Figures S9–S17). In addition, pharmacological correction of NMDAR function in a wrong direction (early D-cycloserine), or during a wrong time window (late memantine), does not normalize social interaction in *Shank2*$^{-/-}$ mice (Figure 5, Supplemental Figures S18 and S20). These results strongly suggest that early NMDAR hyperfunction induces late NMDAR hypofunction and social deficits in *Shank2*$^{-/-}$ mice, and early correction of NMDAR function has long-lasting effects on NMDAR function and social interaction.

Regarding how early memantine treatment induces long-lasting influences on electrophysiology and behavior in *Shank2*$^{-/-}$ mice, it is possible that once the NMDAR function is normalized by early chronic memantine treatment at the juvenile stage, the continuing lack of *Shank2* expression after the end of early memantine treatment period (P7–P21) may not induce a further change in NMDAR function. This hypothesis

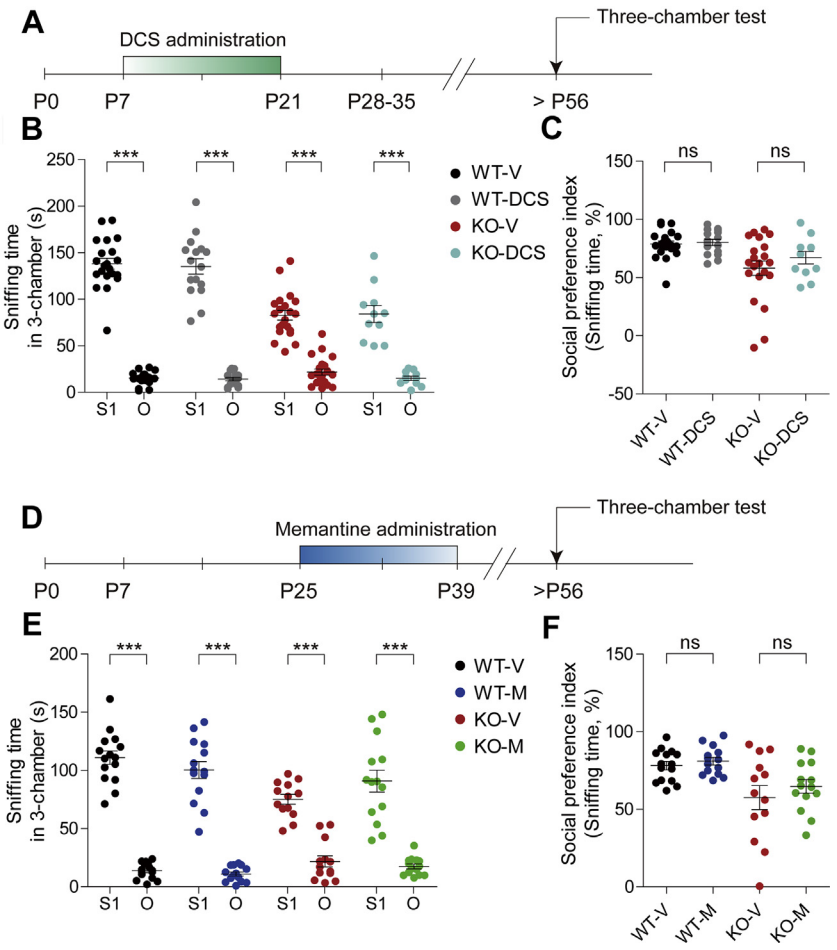

Figure 5. Early D-cycloserine (DCS) or late memantine treatment does not improve social interaction in adult *Shank2*$^{-/-}$ mice. **(A)** Schematic depiction of early D-cycloserine treatment and behavioral tests. Young *Shank2*$^{-/-}$ mice were orally administered D-cycloserine (40 mg/kg) twice daily for 2 weeks during the postnatal day (P)7 to P21 period, followed by consecutive measurements of open-field hyperactivity and three-chamber social interaction during the P56 to P70 period. **(B, C)** Early D-cycloserine treatment fails to improve social interaction of adult *Shank2*$^{-/-}$ mice, as indicated by time sniffing stranger mouse/object (S1/O) and the social preference index based on sniffing time in the three-chamber test. [n = 21 mice for wild-type vehicle (WT-V), 16 mice for WT-memantine (M), 21 mice for knockout (KO)-V, and 11 mice for KO-M; ***$p < .001$, not significant (ns); paired Student's t test or Wilcoxon matched pairs signed rank test **(B)**, Mann-Whitney U test **(C)**.] **(D)** Schematic depiction of late chronic memantine treatment and behavioral tests. *Shank2*$^{-/-}$ mice were orally administered memantine (20 mg/kg) twice daily for 2 weeks during the P25 to P39 period, followed by consecutive measurements of three-chamber social interaction and open-field hyperactivity during the P56 to P90 period. **(E, F)** Late chronic memantine treatment fails to improve social interaction in *Shank2*$^{-/-}$ mice, as indicated by time sniffing S1/O and the social preference index based on sniffing time in the three-chamber test. [n = 15 mice for WT-V, 14 mice for WT-M, 13 mice for KO-V, and 14 mice for KO-M; ***$p < .001$; paired Student's t test or Wilcoxon matched pairs signed rank test **(E)**, unpaired Student's t-test **(F)**.]

could be tested by inducing a *Shank2* KO by a genetic method that starts from ~P21 after the completion of normal brain development during embryonic and early postnatal stages. Our results are reminiscent of a recent report (61) that showed early correction of serotonin levels in infants through mother milk in a mouse model of autism carrying the human 15q11-13 duplication has long-lasting effects, rescuing serotonin levels as well as social behaviors in adults, which, together with our results, strongly suggest that early corrections are important.

Early memantine treatment of WT mice does not affect NMDAR function (Figures 3 and 4). This might be attributable to the fact that the daily and total doses of memantine are in the range that can normalize NMDAR function in *Shank2*$^{-/-}$ mice but that do not suppress the normal NMDAR function in WT mice. Intriguingly, early D-cycloserine treatment of WT mice induces a decrease in NMDAR function at the juvenile stage (Supplemental Figure S19), although it does not affect behaviors at the adult stage (Figure 5A–C). This could be attributable to the fact that the doses of D-cycloserine may be just enough to induce a decrease in NMDAR activity but not enough to impair behaviors in WT mice, which may require a continuing deficit such as *Shank2* KO. Alternatively, D-cycloserine may affect all NMDAR-expressing neurons, whereas *Shank2* KO may mainly affect *Shank2*-expressing neurons.

Our data also provide evidence suggesting that the GluN2B component contributes to the distinct NMDAR functions at P14 and P21 in *Shank2*$^{-/-}$ mouse synapses (Figure 2). Specifically, P14 *Shank2*$^{-/-}$ mouse synapses show markedly increased GluN2B component, whereas P21 *Shank2*$^{-/-}$ mouse synapses show normal levels of GluN2B component. Therefore, the increased NMDAR-mediated currents at P14 may be mainly mediated by GluN2B-containing NMDARs with slower decay kinetics, whereas the decreased NMDAR-mediated currents at P21, where both GluN2A and GluN2B are reduced, may involve both GluN2B-dependent and -independent mechanisms.

Regarding further details, our immunoblot analyses suggest candidate mechanisms involving GluN1/GluN2B phosphorylation (Supplemental Figure S8). It is known that GluN1-Ser896 phosphorylation promotes the endoplasmic reticulum–to–plasma membrane trafficking of GluN1 (62). In addition, calcium/calmodulin-dependent protein kinase II/PKC-dependent GluN2B-Ser1303 phosphorylation promotes synaptic retention of GluN2B through mechanisms involving the binding of GluN2B to MAGUKs (i.e., PSD-95) and activated protein kinase 2–dependent endocytosis of GluN2B (63–66). Therefore, the increased phosphorylation of GluN1-Ser896 and GluN2B-Ser1303 at P14 *Shank2*$^{-/-}$ mouse synapses may

promote surface and synaptic localization of NMDARs, whereas the decreased phosphorylation of GluN1-Ser896 and GluN2B-Ser1303 at P21 *Shank2*$^{-/-}$ mice synapses may suppress synaptic retention of NMDARs. These mechanisms might contribute to the differential contributions of the GluN2B component to NMDAR currents in P14 and P21 *Shank2*$^{-/-}$ mice. However, it should be pointed out that these biochemical changes could reflect those from many different types of cells with some limitations in the interpretation.

Developmental switches of NMDAR function were not observed in other *Shank2*$^{-/-}$ mouse mutant lines. *Shank2*-dEx7 mice show normal NMDAR function at ~P14 but show increased NMDAR function at ~P21, as reported previously (67). In addition, *Shank2*-dEx24 mice showed reduced NMDAR function at ~P21, as reported previously (33), but normal NMDAR function at ~P14, which is partly similar to our mouse line. This discrepancy might be attributable to the differential expression of *Shank2* splice variants in these mouse lines (Figures S25 and S26). For instance, we found a marked difference in the levels of the *SHANK2A* transcript in *Shank2*-dEx6-7 and *Shank2*-dEx7 lines and, by molecular modeling (Supplemental Figure S27), the possibility that a short truncated peptide derived from the *SHANK2A* transcript in *Shank2*-dEx7 mice inhibits the normal interaction between SHANK2 and SAPAPs, which may affect NMDAR activity or signaling, in a dominant-negative manner, although the presence of such short peptides could not be directly determined by immunoblot analyses. In addition, the exon 24 deleted in *Shank2*-dEx24 mice encodes the proline-rich region containing the Homer- and cortactin-binding sites (33), which are known to mediate the formation of a polymeric network structure and regulate the actin cytoskeleton in the postsynaptic density (68,69). Although further details remain to be studied, these results are at the very least in line with the finding that, in humans, different *SHANK2* mutations, in other words, exons 6 and 7 and exon 7 deletions, are associated with distinct ASD symptoms (37). Similarly, two different mutations of *SHANK3* (a *SHANK2* relative) from ASD and patients with schizophrenia, respectively, cause ASD- and schizophrenia-like phenotypes in mice (70).

NMDAR dysfunction, which would suppress normal brain development and function, has been suggested as an important candidate mechanism that may underlie ASD (71). Disturbances in NMDAR function, as a subset of excitatory synaptic function, would also induce the imbalance between synaptic and neuronal excitation and inhibition, another key mechanism implicated in ASD (72,73). Given that NMDAR function is an important target for dynamic regulation and fine-tuning for normal brain development and function (53,74), our results suggest that NMDAR dysfunctions observed in many other animal models of ASD (71,75–90) may need to be further examined for their temporal changes. This might eventually help us develop more cautious treatment strategies for patients who have ASD with distinct temporal patterns of NMDAR dysfunctions.

In conclusion, our results suggest that *Shank2* deletion in mice leads to NMDAR hyperfunction at an early stage that is causally associated with NMDAR hypofunction and social deficits at later stages. In addition, our study suggests that early correction of NMDAR hyperfunction in *Shank2*$^{-/-}$ mice has long-lasting effects, preventing synaptic and social abnormalities from manifesting at later stages.

ACKNOWLEDGMENTS AND DISCLOSURES

This work was supported by the National Research Foundation (NRF) (Grant No. NRF-2013M3C7A1056732 [to HyuKi]), NRF-2013-Fostering Core Leaders of the Future Basic Science Program (Grant No. NRF-2013H1A8A1004150 [to CC]), Global Ph.D. Fellowship Program (Grant No. NRF-2013H1A2A1032785 [to SH] and Grant No. NRF-2015H1A2A1033937 [to RK]), the National Honor Scientist Program (Grant No. NRF-2012R1A3A1050385 [to B-KK]), the National Institute of Health grants (Grant Nos. MH098114, MH104316, and HD087795 [to Y-hJ]), Korea Institute of Science and Technology Information (Grant No. K-17-L03-C02-S01 [to HKa]), and the Institute for Basic Science (Grant No. IBS-R002-D1 [to EK]).

The authors report no biomedical financial interests or potential conflicts of interest.

ARTICLE INFORMATION

From the Department of Biological Sciences (CC, SH, SMU, Y-EY, TY, SL, RK, YK, WK, HyoKi, EK) and Department of Mathematical Sciences (YC), Korea Advanced Institute for Science and Technology; Center for Synaptic Brain Dysfunctions (CC, JL, HJ, DL, EL, JK, DK, EK), Institute for Basic Science; and Department of Convergence Technology Research (HKa), Korea Institute of Science and Technology Information, Daejeon; Department of Anatomy and Neurobiology (WM), School of Dentistry, Kyungpook National University, Daegu; Department of Anatomy and Division of Brain Korea 21 (SM, JYK, HyuKi), Biomedical Science, College of Medicine, Korea University; and School of Biological Sciences (C-SL, B-KK), Seoul National University, Seoul, South Korea; Department of Pediatrics (HY, LD, Y-hJ), Department of Neurobiology (Y-hJ), Cell and Molecular Biology Program (Y-hJ), Duke Institute of Brain Science (Y-hJ), and Genomics and Genetics Program (Y-hJ), Duke University, Durham, North Carolina; Department of Neurology (HW), Center for Autism Research and Treatment, Semel Institute, David Geffen School of Medicine, University of California Los Angeles, Los Angeles, California; and the Institute for Anatomy and Cell Biology (TMB), Ulm University, Ulm, Germany.

WM and HW are currently affiliated with the Department of Genetics and University of North Carolina Neuroscience Center, University of North Carolina, Chapel Hill, North Carolina. C-SL is currently affiliated with the Department of Pharmacology, Wonkwang University School of Medicine, Iksan, South Korea.

CC and SH contributed equally to this work.

Address correspondence to Eunjoon Kim, Ph.D., Korea Advanced Institute for Science and Technology, Department of Biological Sciences, Daejeon 305 701, Republic of Korea; E-mail: kime@kaist.ac.kr, or eunjoonkim1@gmail.com.

Received Jul 26, 2018; revised Sep 20, 2018; accepted Sep 26, 2018.

Supplementary material cited in this article is available online at https://doi.org/10.1016/j.biopsych.2018.09.025.

REFERENCES

1. Abrahams BS, Arking DE, Campbell DB, Mefford HC, Morrow EM, Weiss LA, *et al.* (2013): SFARI Gene 2.0: a community-driven knowledgebase for the autism spectrum disorders (ASDs). Mol Autism 4:36.
2. Sudhof TC (2008): Neuroligins and neurexins link synaptic function to cognitive disease. Nature 455:903–911.
3. Zoghbi HY, Bear MF (2012): Synaptic dysfunction in neurodevelopmental disorders associated with autism and intellectual disabilities. Cold Spring Harb Perspect Biol 4:a009886.
4. Jiang YH, Ehlers MD (2013): Modeling autism by SHANK gene mutations in mice. Neuron 78:8–27.
5. Bourgeron T (2015): From the genetic architecture to synaptic plasticity in autism spectrum disorder. Nat Rev Neurosci 16:551–563.
6. de la Torre-Ubieta L, Won H, Stein JL, Geschwind DH (2016): Advancing the understanding of autism disease mechanisms through genetics. Nat Med 22:345–361.
7. Sala C, Vicidomini C, Bigi I, Mossa A, Verpelli C (2015): Shank synaptic scaffold proteins: keys to understanding the pathogenesis of autism and other synaptic disorders. J Neurochem 135:849–858.

8. Volk L, Chiu SL, Sharma K, Huganir RL (2015): Glutamate synapses in human cognitive disorders. Annu Rev Neurosci 38:127–149.
9. Ehninger D, Silva AJ (2011): Rapamycin for treating tuberous sclerosis and autism spectrum disorders. Trends Mol Med 17:78–87.
10. Kaiser T, Feng G (2015): Modeling psychiatric disorders for developing effective treatments. Nat Med 21:979–988.
11. Kleijer KT, Schmeisser MJ, Krueger DD, Boeckers TM, Scheiffele P, Bourgeron T, *et al.* (2014): Neurobiology of autism gene products: towards pathogenesis and drug targets. Psychopharmacology 231:1037–1062.
12. Aceti M, Creson TK, Vaissiere T, Rojas C, Huang WC, Wang YX, *et al.* (2015): Syngap1 haploinsufficiency damages a postnatal critical period of pyramidal cell structural maturation linked to cortical circuit assembly. Biol Psychiatry 77:805–815.
13. Clement JP, Aceti M, Creson TK, Ozkan ED, Shi Y, Reish NJ, *et al.* (2012): Pathogenic SYNGAP1 mutations impair cognitive development by disrupting maturation of dendritic spine synapses. Cell 151:709–723.
14. Sheng M, Hoogenraad CC (2007): The postsynaptic architecture of excitatory synapses: A more quantitative view. Annu Rev Biochem 76:823–847.
15. Sheng M, Kim E (2011): The postsynaptic organization of synapses. Cold Spring Harb Perspect Biol 3:a005678.
16. Mossa A, Giona F, Pagano J, Sala C, Verpelli C (2017): SHANK genes in autism: Defining therapeutic targets. Prog Neuropsychopharmacol Biol Psychiatry 84:416–423.
17. Monteiro P, Feng G (2017): SHANK proteins: Roles at the synapse and in autism spectrum disorder. Nat Rev Neurosci 18:147–157.
18. Leblond CS, Heinrich J, Delorme R, Proepper C, Betancur C, Huguet G, *et al.* (2012): Genetic and functional analyses of SHANK2 mutations suggest a multiple hit model of autism spectrum disorders. PLoS Genet 8:e1002521.
19. Berkel S, Tang W, Trevino M, Vogt M, Obenhaus HA, Gass P, *et al.* (2012): Inherited and de novo SHANK2 variants associated with autism spectrum disorder impair neuronal morphogenesis and physiology. Hum Mol Genet 21:344–357.
20. Schluth-Bolard C, Labalme A, Cordier MP, Till M, Nadeau G, Tevissen H, *et al.* (2013): Breakpoint mapping by next generation sequencing reveals causative gene disruption in patients carrying apparently balanced chromosome rearrangements with intellectual deficiency and/or congenital malformations. J Med Genet 50:144–150.
21. Prasad A, Merico D, Thiruvahindrapuram B, Wei J, Lionel AC, Sato D, *et al.* (2012): A discovery resource of rare copy number variations in individuals with autism spectrum disorder. G3 (Bethesda) 2:1665–1685.
22. Sanders SJ, Murtha MT, Gupta AR, Murdoch JD, Raubeson MJ, Willsey AJ, *et al.* (2012): De novo mutations revealed by whole-exome sequencing are strongly associated with autism. Nature 485: 237–241.
23. Pinto D, Pagnamenta AT, Klei L, Anney R, Merico D, Regan R, *et al.* (2010): Functional impact of global rare copy number variation in autism spectrum disorders. Nature 466:368–372.
24. Chilian B, Abdollahpour H, Bierhals T, Haltrich I, Fekete G, Nagel I, *et al.* (2013): Dysfunction of SHANK2 and CHRNA7 in a patient with intellectual disability and language impairment supports genetic epistasis of the two loci. Clin Genet 84:560–565.
25. Leblond CS, Nava C, Polge A, Gauthier J, Huguet G, Lumbroso S, *et al.* (2014): Meta-analysis of SHANK mutations in autism spectrum disorders: a gradient of severity in cognitive impairments. PLoS Genet 10:e1004580.
26. Rauch A, Wieczorek D, Graf E, Wieland T, Endele S, Schwarzmayr T, *et al.* (2012): Range of genetic mutations associated with severe non-syndromic sporadic intellectual disability: An exome sequencing study. Lancet 380:1674–1682.
27. Wischmeijer A, Magini P, Giorda R, Gnoli M, Ciccone R, Cecconi L, *et al.* (2011): Olfactory receptor-related duplicons mediate a microdeletion at 11q13.2q13.4 associated with a syndromic phenotype. Mol Syndromol 1:176–184.
28. Peykov S, Berkel S, Degenhardt F, Rietschel M, Nothen MM, Rappold GA (2015): Rare SHANK2 variants in schizophrenia. Mol Psychiatry 20:1487–1488.
29. Peykov S, Berkel S, Schoen M, Weiss K, Degenhardt F, Strohmaier J, *et al.* (2015): Identification and functional characterization of rare SHANK2 variants in schizophrenia. Mol Psychiatry 20:1489–1498.
30. Homann OR, Misura K, Lamas E, Sandrock RW, Nelson P, McDonough SI, *et al.* (2016): Whole-genome sequencing in multiplex families with psychoses reveals mutations in the SHANK2 and SMARCA1 genes segregating with illness. Mol Psychiatry 21:1690–1695.
31. Costas J (2015): The role of SHANK2 rare variants in schizophrenia susceptibility. Mol Psychiatry 20:1486.
32. Kim R, Kim J, Chung C, Ha S, Lee S, Lee E, *et al.* (2018): Cell-type-specific Shank2 deletion in mice leads to differential synaptic and behavioral phenotypes. J Neurosci 38:4076–4092.
33. Pappas AL, Bey AL, Wang X, Rossi M, Kim YH, Yan H, *et al.* (2017): Deficiency of Shank2 causes mania-like behavior that responds to mood stabilizers. JCI Insight 2:92052.
34. Lim CS, Kim H, Yu NK, Kang SJ, Kim T, Ko HG, *et al.* (2017): Enhancing inhibitory synaptic function reverses spatial memory deficits in Shank2 mutant mice. Neuropharmacology 112:104–112.
35. Ha S, Lee D, Cho YS, Chung C, Yoo YE, Kim J, *et al.* (2016): Cerebellar Shank2 regulates excitatory synapse density, motor coordination, and specific repetitive and anxiety-like behaviors. J Neurosci 36:12129–12143.
36. Peter S, Ten Brinke MM, Stedehouder J, Reinelt CM, Wu B, Zhou H, *et al.* (2016): Dysfunctional cerebellar Purkinje cells contribute to autism-like behaviour in Shank2-deficient mice. Nat Commun 7:12627.
37. Schmeisser MJ, Ey E, Wegener S, Bockmann J, Stempel V, Kuebler A, *et al.* (2012): Autistic-like behaviours and hyperactivity in mice lacking ProSAP1/Shank2. Nature 486:256–260.
38. Won H, Lee HR, Gee HY, Mah W, Kim JI, Lee J, *et al.* (2012): Autistic-like social behaviour in Shank2-mutant mice improved by restoring NMDA receptor function. Nature 486:261–265.
39. Heise C, Preuss JM, Schroeder JC, Battaglia CR, Kolibius J, Schmid R, *et al.* (2018): Heterogeneity of cell surface glutamate and GABA receptor expression in Shank and CNTN4 autism mouse models. Front Mol Neurosci 11:212.
40. Lee S, Lee E, Kim R, Kim J, Lee S, Park H, *et al.* (2018): Shank2 deletion in parvalbumin neurons leads to moderate hyperactivity, enhanced self-grooming and suppressed seizure susceptibility in mice. Front Mol Neurosci 11:209.
41. Ey E, Torquet N, Le Sourd AM, Leblond CS, Boeckers TM, Faure P, *et al.* (2013): The autism ProSAP1/Shank2 mouse model displays quantitative and structural abnormalities in ultrasonic vocalisations. Behav Brain Res 256:677–689.
42. Sato M, Kawano M, Mizuta K, Islam T, Lee MG, Hayashi Y (2017): Hippocampus-dependent goal localization by head-fixed mice in virtual reality. eNeuro 4:ENEURO.0369-16.2017.
43. Yoon SY, Kwon SG, Kim YH, Yeo JH, Ko HG, Roh DH, *et al.* (2017): A critical role of spinal Shank2 proteins in NMDA-induced pain hypersensitivity. Mol Pain 13:1744806916688902.
44. Ferhat AT, Torquet N, Le Sourd AM, de Chaumont F, Olivo-Marin JC, Faure P, *et al.* (2016): Recording mouse ultrasonic vocalizations to evaluate social communication. J Vis Exp (112), e53871.
45. Ko HG, Oh SB, Zhuo M, Kaang BK (2016): Reduced acute nociception and chronic pain in Shank2-/- mice. Mol Pain 12:1744806916647056.
46. Zuo Y, Lin A, Chang P, Gan WB (2005): Development of long-term dendritic spine stability in diverse regions of cerebral cortex. Neuron 46:181–189.
47. Subramanian A, Tamayo P, Mootha VK, Mukherjee S, Ebert BL, Gillette MA, *et al.* (2005): Gene set enrichment analysis: A knowledge-based approach for interpreting genome-wide expression profiles. Proc Natl Acad Sci U S A 102:15545–15550.
48. Subramanian A, Kuehn H, Gould J, Tamayo P, Mesirov JP (2007): GSEA-P: A desktop application for Gene Set Enrichment Analysis. Bioinformatics 23:3251–3253.
49. Schumann CM, Hamstra J, Goodlin-Jones BL, Lotspeich LJ, Kwon H, Buonocore MH, *et al.* (2004): The amygdala is enlarged in children but

not adolescents with autism; the hippocampus is enlarged at all ages. J Neurosci 24:6392–6401.
50. Endo T, Shioiri T, Kitamura H, Kimura T, Endo S, Masuzawa N, *et al.* (2007): Altered chemical metabolites in the amygdala-hippocampus region contribute to autistic symptoms of autism spectrum disorders. Biol Psychiatry 62:1030–1037.
51. Felix-Ortiz AC, Tye KM (2014): Amygdala inputs to the ventral hippocampus bidirectionally modulate social behavior. J Neurosci 34:586–595.
52. Yizhar O, Fenno LE, Prigge M, Schneider F, Davidson TJ, O'Shea DJ, *et al.* (2011): Neocortical excitation/inhibition balance in information processing and social dysfunction. Nature 477:171–178.
53. Lussier MP, Sanz-Clemente A, Roche KW (2015): Dynamic regulation of N-methyl-d-aspartate (NMDA) and alpha-amino-3-hydroxy-5-methyl-4-isoxazolepropionic acid (AMPA) receptors by post-translational modifications. J Biol Chem 290:28596–28603.
54. Yang M, Silverman JL, Crawley JN (2011): Automated three-chambered social approach task for mice. Curr Protoc Neurosci. Chapter 8:Unit 8.26.
55. Silverman JL, Yang M, Lord C, Crawley JN (2010): Behavioural phenotyping assays for mouse models of autism. Nat Rev Neurosci 11:490–502.
56. Ferguson JN, Young LJ, Hearn EF, Matzuk MM, Insel TR, Winslow JT (2000): Social amnesia in mice lacking the oxytocin gene. Nat Genet 25:284–288.
57. Wang F, Zhu J, Zhu H, Zhang Q, Lin Z, Hu H (2011): Bidirectional control of social hierarchy by synaptic efficacy in medial prefrontal cortex. Science 334:693–697.
58. Yang M, Lewis F, Foley G, Crawley JN (2015): In tribute to Bob Blanchard: Divergent behavioral phenotypes of 16p11.2 deletion mice reared in same-genotype versus mixed-genotype cages. Physiol Behav 146:16–27.
59. Spencer CM, Alekseyenko O, Serysheva E, Yuva-Paylor LA, Paylor R (2005): Altered anxiety-related and social behaviors in the Fmr1 knockout mouse model of fragile X syndrome. Genes Brain Behav 4:420–430.
60. Kalbassi S, Bachmann SO, Cross E, Roberton VH, Baudouin SJ (2017): Male and female mice lacking neuroligin-3 modify the behavior of their wild-type littermates. eNeuro 4:ENEURO.0145-17.2017.
61. Nakai N, Nagano M, Saitow F, Watanabe Y, Kawamura Y, Kawamoto A, *et al.* (2017): Serotonin rebalances cortical tuning and behavior linked to autism symptoms in 15q11-13 CNV mice. Sci Adv 3:e1603001.
62. Scott DB, Blanpied TA, Swanson GT, Zhang C, Ehlers MD (2001): An NMDA receptor ER retention signal regulated by phosphorylation and alternative splicing. J Neurosci 21:3063–3072.
63. Sanz-Clemente A, Gray JA, Ogilvie KA, Nicoll RA, Roche KW (2013): Activated CaMKII couples GluN2B and casein kinase 2 to control synaptic NMDA receptors. Cell Rep 3:607–614.
64. Lavezzari G, McCallum J, Lee R, Roche KW (2003): Differential binding of the AP-2 adaptor complex and PSD-95 to the C-terminus of the NMDA receptor subunit NR2B regulates surface expression. Neuropharmacology 45:729–737.
65. Prybylowski K, Chang K, Sans N, Kan L, Vicini S, Wenthold RJ (2005): The synaptic localization of NR2B-containing NMDA receptors is controlled by interactions with PDZ proteins and AP-2. Neuron 47:845–857.
66. Sanz-Clemente A, Matta JA, Isaac JT, Roche KW (2010): Casein kinase 2 regulates the NR2 subunit composition of synaptic NMDA receptors. Neuron 67:984–996.
67. Schmeisser MJ (2015): Translational neurobiology in Shank mutant mice—model systems for neuropsychiatric disorders. Ann Anat 200:115–117.
68. Hayashi MK, Tang C, Verpelli C, Narayanan R, Stearns MH, Xu RM, *et al.* (2009): The postsynaptic density proteins Homer and Shank form a polymeric network structure. Cell 137:159–171.
69. Naisbitt S, Kim E, Tu JC, Xiao B, Sala C, Valtschanoff J, *et al.* (1999): Shank, a novel family of postsynaptic density proteins that binds to the NMDA receptor/PSD-95/GKAP complex and cortactin. Neuron 23:569–582.
70. Zhou Y, Kaiser T, Monteiro P, Zhang X, Van der Goes MS, Wang D, *et al.* (2016): Mice with Shank3 mutations associated with ASD and schizophrenia display both shared and distinct defects. Neuron 89:147–162.
71. Lee EJ, Choi SY, Kim E (2015): NMDA receptor dysfunction in autism spectrum disorders. Curr Opin Pharmacol 20C:8–13.
72. Lee E, Lee J, Kim E (2017): Excitation/inhibition imbalance in animal models of autism spectrum disorders. Biol Psychiatry 81:838–847.
73. Nelson SB, Valakh V (2015): Excitatory/inhibitory balance and circuit homeostasis in autism spectrum disorders. Neuron 87:684–698.
74. Paoletti P, Bellone C, Zhou Q (2013): NMDA receptor subunit diversity: Impact on receptor properties, synaptic plasticity and disease. Nat Rev Neurosci 14:383–400.
75. Blundell J, Blaiss CA, Etherton MR, Espinosa F, Tabuchi K, Walz C, *et al.* (2010): Neuroligin-1 deletion results in impaired spatial memory and increased repetitive behavior. J Neurosci 30:2115–2129.
76. Chung W, Choi SY, Lee E, Park H, Kang J, Park H, *et al.* (2015): Social deficits in IRSp53 mutant mice improved by NMDAR and mGluR5 suppression. Nat Neurosci 18:435–443.
77. Huang TN, Chuang HC, Chou WH, Chen CY, Wang HF, Chou SJ, *et al.* (2014): Tbr1 haploinsufficiency impairs amygdalar axonal projections and results in cognitive abnormality. Nat Neurosci 17:240–247.
78. Lee EJ, Lee H, Huang TN, Chung C, Shin W, Kim K, *et al.* (2015): Trans-synaptic zinc mobilization improves social interaction in two mouse models of autism through NMDAR activation. Nat Commun 6:7168.
79. Duffney LJ, Wei J, Cheng J, Liu W, Smith KR, Kittler JT, *et al.* (2013): Shank3 deficiency induces NMDA receptor hypofunction via an actin-dependent mechanism. J Neurosci 33:15767–15778.
80. Duffney LJ, Zhong P, Wei J, Matas E, Cheng J, Qin L, *et al.* (2015): Autism-like deficits in Shank3-deficient mice are rescued by targeting actin regulators. Cell Rep 11:1400–1413.
81. Jaramillo TC, Liu S, Pettersen A, Birnbaum SG, Powell CM (2014): Autism-related neuroligin-3 mutation alters social behavior and spatial learning. Autism Res 7:264–272.
82. Kouser M, Speed HE, Dewey CM, Reimers JM, Widman AJ, Gupta N, *et al.* (2013): Loss of predominant Shank3 isoforms results in hippocampus-dependent impairments in behavior and synaptic transmission. J Neurosci 33:18448–18468.
83. Rinaldi T, Kulangara K, Antoniello K, Markram H (2007): Elevated NMDA receptor levels and enhanced postsynaptic long-term potentiation induced by prenatal exposure to valproic acid. Proc Natl Acad Sci U S A 104:13501–13506.
84. Kang J, Kim E (2015): Suppression of NMDA receptor function in mice prenatally exposed to valproic acid improves social deficits and repetitive behaviors. Front Mol Neurosci 8:17.
85. Kim KC, Lee DK, Go HS, Kim P, Choi CS, Kim JW, *et al.* (2014): Pax6-dependent cortical glutamatergic neuronal differentiation regulates autism-like behavior in prenatally valproic acid-exposed rat offspring. Mol Neurobiol 49:512–528.
86. Takeuchi K, Gertner MJ, Zhou J, Parada LF, Bennett MV, Zukin RS (2013): Dysregulation of synaptic plasticity precedes appearance of morphological defects in a Pten conditional knockout mouse model of autism. Proc Natl Acad Sci U S A 110:4738–4743.
87. Jaramillo TC, Speed HE, Xuan Z, Reimers JM, Liu S, Powell CM (2016): Altered striatal synaptic function and abnormal behaviour in Shank3 exon4-9 deletion mouse model of autism. Autism Res 9:350–375.
88. Speed HE, Kouser M, Xuan Z, Reimers JM, Ochoa CF, Gupta N, *et al.* (2015): Autism-associated insertion mutation (InsG) of Shank3 exon 21 causes impaired synaptic transmission and behavioral deficits. J Neurosci 35:9648–9665.
89. Espinosa F, Xuan Z, Liu S, Powell CM (2015): Neuroligin 1 modulates striatal glutamatergic neurotransmission in a pathway and NMDAR subunit-specific manner. Front Synaptic Neurosci 7:11.
90. Bozdagi O, Sakurai T, Papapetrou D, Wang X, Dickstein DL, Takahashi N, *et al.* (2010): Haploinsufficiency of the autism-associated Shank3 gene leads to deficits in synaptic function, social interaction, and social communication. Mol Autism 1:15.